

Unveiling Higher-Order Topology via Polarized Topological Charges

Wei Jia,¹ Bao-Zong Wang,² Ming-Jian Gao,¹ and Jun-Hong An^{1,*}

¹Key Laboratory of Quantum Theory and Applications of MoE, Lanzhou Center for Theoretical Physics, and Key Laboratory of Theoretical Physics of Gansu Province, Lanzhou University, Lanzhou 730000, China

²International Center for Quantum Materials, School of Physics, Peking University, Beijing 100871, China

Real-space topological invariants were widely used to characterize chiral-symmetric higher-order topological phases (HOTPs). However, a momentum-space characterization to these HOTPs, which essentially reveals their intrinsic bulk-boundary correspondence and facilitates their detection in quantum simulation systems, is still lacking. Here, we propose an experimentally observable momentum-space characterization to the chiral-symmetric HOTPs by the concept of polarized topological charges. It makes a unified description to the HOTPs caused by the closing and reopening of band gap not only of the bulk states but also the edge states. Remarkably, these polarized topological charges can also be identified by measuring the pseudospin structures. A feasible scheme to detect the HOTPs in the ^{87}Rb atomic system is given. Our work opens an avenue for characterization and experimental detection of the HOTPs in momentum space.

Introduction.—Topological phases of matter have generated great interest in the past decades. Recently, higher-order topological phases (HOTPs) have generalized the well-known bulk-boundary correspondence (BBC) such that a n th-order topological phase in d -dimensional (d D) systems hosts $(d-n)$ D gapless boundary states [1–5]. This nontrivial correspondence endows HOTPs with a key feature of rich topological states [6–21] and induces their potential applications in quantum computation [22] and quantum interferometer [23]. Currently, a variety of HOTPs have been discovered in insulators [24–35], semimetals [36–43], and superconductors [44–51]. The studies have also been extended in Floquet [52–54], non-Hermitian [55–58], interacting [59, 60], and fractal systems [61, 62]. Due to the sophisticated topological origins rooted in bulk or boundary of the higher-order topological systems, a fundamental issue is how to exactly characterize and detect the HOTPs.

For chiral-symmetric HOTPs of the Altland-Zirnbauer tenfold classification [63–66], the real-space topological invariants such as multipole chiral numbers (MCNs) [67], multipole winding numbers [68], and Bott indices [69] have pioneered the novel insights in their topological characterizations, which also reveals the exotic topological states protecting multiple zero modes at each corner. Further, these topological corner states have been observed by simulating boundary physics of the lattices via the classical systems, such as acoustic crystals [70, 71] and electric circuits [72]. Nevertheless, these topological invariants describe the chiral-symmetric HOTPs from real-space physics and cannot completely reveal the BBC. The reason is that the bulk topology is defined by the eigenstates of Bloch Hamiltonian in the Brillouin zone (BZ) in principle [73, 74]. It makes the topological invariants defined in momentum space the only essential reflection of the BBC. Yet, this momentum-space topological invariant describing the chiral-symmetric HOTPs is still lacking. On the other hand, the real-space topological invariants have complex mathematical forms and are dif-

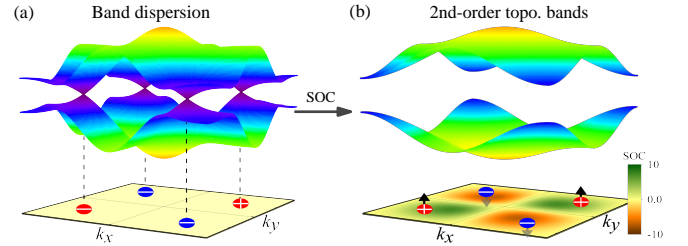


FIG. 1. (a) Band dispersion without the SO coupling give four nodal points with positive or negative unit-value topological charges. (b) SO coupling opens band gap and causes the topological charges to be polarized. The polarization $\mathcal{P}_n = +1$ and -1 are marked by arrows parallel and antiparallel to the direction $\mathbf{k}_x \times \mathbf{k}_y$, respectively. A quarter of total polarized topological charges determines the second-order topology.

ficult to directly measure in realistic experiments. Meanwhile, the real-space characterizations are not conducive to detect these HOTPs in quantum simulation systems with high controllability, such as ultracold atoms [75–78], nitrogen-vacancy center [79–81], and nuclear magnetic resonance [82, 83], as the bulk physics are conveniently simulated in these artificial systems. Hence, there is an urgent need for an experimentally observable momentum-space topological characterization of chiral-symmetric HOTPs to reveal the BBC and further promote the quantum simulations.

In this Letter, we propose a concept of polarized topological charges in momentum space to characterize the chiral-symmetric HOTPs and an experimental scheme to detect the HOTPs based on ^{87}Rb atomic system [84]. Our characterization theory covers different topological classifications and has broad applications. It is revealed that the topological charges defined in the band dispersion are polarized by the pseudospin-orbit coupling of the topological systems. The second-order (third-order) topological phases are well determined by a quarter (negative eighth) of the total polarized topological charges.

The topological phase transitions, induced by the closing and reopening of band gap not only of the bulk states but also the edge states, can be uniformly characterized by the changes of polarized topological charges. We also show that these polarized topological charges can be determined by observing the expectation values of the pseudospins. Our work elegantly interprets the BBC of the HOTPs and would stimulate the experimental detection of HOTPs in quantum simulation platforms.

2D generic theory.—We first focus on a family of 2D lattice systems that host chiral-symmetric second-order topological phases. The minimal momentum-space Hamiltonian to satisfy this requirement reads

$$\mathcal{H}(\mathbf{k}) = \sum_{i=1}^4 h_i(\mathbf{k}) \Gamma_i. \quad (1)$$

The Gamma matrices obeying $\{\Gamma_i, \Gamma_j\} = 2\delta_{ij}$ are of dimensionality 4 (classes AIII and BDI) or 8 (class CII) [85, 86], which guarantees that there is a chiral operator Γ_5 to satisfy $\Gamma_5 \mathcal{H}(\mathbf{k}) \Gamma_5 = -\mathcal{H}(\mathbf{k})$. We here arrange the Gamma matrices in an order satisfying the trace property $\text{Tr}(\Gamma_5 \Gamma_1 \Gamma_2 \Gamma_3 \Gamma_4) = -4$ [87, 88]. Hence our systems have chiral symmetry and possess \mathbb{Z} -classified second-order topological phases [1, 2, 12, 13, 16, 67, 85, 86].

Inspired by the description of first-order topology [89–92], we resort to the so-called topological charge defined in the momentum space to characterize the second-order topological phases. Specifically, we separate $\mathbf{h}(\mathbf{k})$ in Eq. (1) into two parts, i.e., $\mathbf{h}(\mathbf{k}) = (\mathbf{h}_m, \mathbf{h}_{so})$, where $\mathbf{h}_m = (h_1, h_2)$ describes the band dispersion and $\mathbf{h}_{so} = (h_3, h_4)$ plays a similar role as the pseudospin-orbit (SO) coupling. In the absence of \mathbf{h}_{so} , there are two gapless energy bands [see Fig. 1(a)]. The n th nodal point \mathbf{q}_n is determined by $\mathbf{h}_m(\mathbf{q}_n) = 0$. A topological charge at \mathbf{q}_n is then defined as

$$\mathcal{C}_n = \text{sgn}\{\det[\partial h_{m,i}(\mathbf{q}_n)/\partial k_j]\}, \quad (2)$$

which describes the winding of \mathbf{h}_m around \mathbf{q}_n . The presence of \mathbf{h}_{so} opens an energy gap. We can endow the charge of \mathbf{q}_n with a polarization [see Fig. 1(b)],

$$\mathcal{P}_n = \text{sgn}[h_3(\mathbf{q}_n)h_4(\mathbf{q}_n)]. \quad (3)$$

The topological invariant of our system is defined as a quarter of total polarized topological charges in the BZ

$$W = \frac{1}{4} \sum_n \mathcal{C}_n \mathcal{P}_n, \quad (4)$$

which provides a momentum-space characterization to the 2D second-order topological phases. In the topologically nontrivial regime, each nodal point has a nonzero \mathcal{C}_n and \mathcal{P}_n , which contributes a nontrivial W [see Fig. 2(a)]. With changing system parameters, the bulk- or edge-state band gap closes. The new (original) topological

charges are created (annihilated) in the zero polarization regions. This causes an abrupt change of W and signifies the emergence of topological phase transitions, as we show it in Figs. 2(c) and 2(d).

The topological invariant W is actually an extension of 1D winding number. To demonstrate this result, we first consider a Su–Schrieffer–Heeger (SSH) chain along x direction. The corresponding momentum-space Hamiltonian reads $\mathcal{H}(k_x) = h_1(k_x)\tau_x + h_3(k_x)\tau_y$ and has chiral symmetry under the chiral operator τ_z , where $\tau_{x,y,z}$ are Pauli matrices. One can define a 1D winding number $W_x = (1/2\pi i) \int_{\text{BZ}} \text{Tr}[q(k_x)^\dagger \partial_{k_x} q(k_x)] dk_x$, with $q(k_x) = h_1(k_x) + i h_3(k_x)$, to characterize its first-order topology [66]. Remarkably, we find that this winding number equals exactly to $W_x = (-1/2) \sum_{l_x=1}^{N_x} \mathcal{C}_{l_x}^x \mathcal{P}_{l_x}^x$ [93], where $\mathcal{C}_{l_x}^x = \text{sgn}[\partial h_1(\varrho_{l_x})/\partial k_x]$ are the topological charges, $\mathcal{P}_{l_x}^x = \text{sgn}[h_3(\varrho_{l_x})]$ are the charge polarizations, and N_x is the number of the nodal points. When a y -directional SSH chain described by $\mathcal{H}(k_y) = h_2(k_y)\sigma_x + h_4(k_y)\sigma_y$, which possesses a similar winding number W_y to W_x , is further stacked to $\mathcal{H}(k_x)$, we obtain a special 2D system described by $\mathcal{H}(k_x, k_y) = \mathcal{H}(k_x) \otimes 1 + \tau_z \otimes \mathcal{H}(k_y)$, whose variables k_x and k_y are separable. Being equivalent to the Benalcazar–Bernevig–Hughes (BBH) model [1, 4], it hosts the chiral-symmetric second-order topological phases. According to Ref. [94], its second-order topology is characterized by $W = W_x W_y$, which is just Eq. (4) by redefining the topological charges $\mathcal{C}_n = \mathcal{C}_{l_x}^x \mathcal{C}_{l_y}^y$ and their polarizations $\mathcal{P}_n = \mathcal{P}_{l_x}^x \mathcal{P}_{l_y}^y$ for the nodal points $\mathbf{q}_n = (\varrho_{l_x}, \varrho_{l_y})$, where $l_{x/y} = 1, \dots, N_{x/y}$ and $n = 1, \dots, N_x N_y$. We further generalize this characterization to generic separable systems, whose topological charges and charge polarizations are generalized to Eq. (2) and Eq. (3), respectively [93]. Remarkably, our scheme can be used in the 2D inseparable systems $\mathcal{H}(\mathbf{k})$ possessing mirror-rotation symmetry [93]. Their second-order topology is described by $\mathcal{H}(k)$ on its high-symmetric lines $k_x = k_y = k$ [58], which is obviously separable. It implies that W is still applicable in these inseparable systems. This result has been verified by the second numerical example presented later. Therefore, we provide an elegant characterization for the second-order topology of 2D systems.

Measurements and applications.—The above topological invariant W is observable by measuring the expectation values $\langle \Gamma_i(\mathbf{k}) \rangle = \langle u(\mathbf{k}) | \Gamma_i | u(\mathbf{k}) \rangle$, where $|u(\mathbf{k})\rangle$ is the ground state of $\mathcal{H}(\mathbf{k})$. We define a pseudospin field $\Theta(\mathbf{k})$, whose component is $\Theta_i(\mathbf{k}) = -\langle \Gamma_i(\mathbf{k}) \rangle / \mathcal{N}_{\mathbf{k}}$, with $i = 1, 2$ and $\mathcal{N}_{\mathbf{k}}$ being a normalization factor. Using the anticommutation relation of Γ , we obtain $\langle \Gamma_i(\mathbf{k}) \rangle = -h_i / (\sum_{i=1}^4 h_i^2)^{1/2}$. It readily leads to $\mathcal{P}_n = \text{sgn}[\langle \Gamma_3(\mathbf{q}_n) \rangle \langle \Gamma_4(\mathbf{q}_n) \rangle]$ and $\Theta(\mathbf{q}_n) = \mathbf{h}_m(\mathbf{q}_n)$. The topological charge \mathcal{C}_n is recast into the winding of $\Theta(\mathbf{k})$ around the nodal points \mathbf{q}_n , which reads $\mathcal{C}_n = \text{sgn}\{\det[\partial \Theta_i(\mathbf{q}_n)/\partial k_j]\}$. Therefore, the topological invariant W is determined by measuring $\langle \Gamma_i(\mathbf{k}) \rangle$, which is

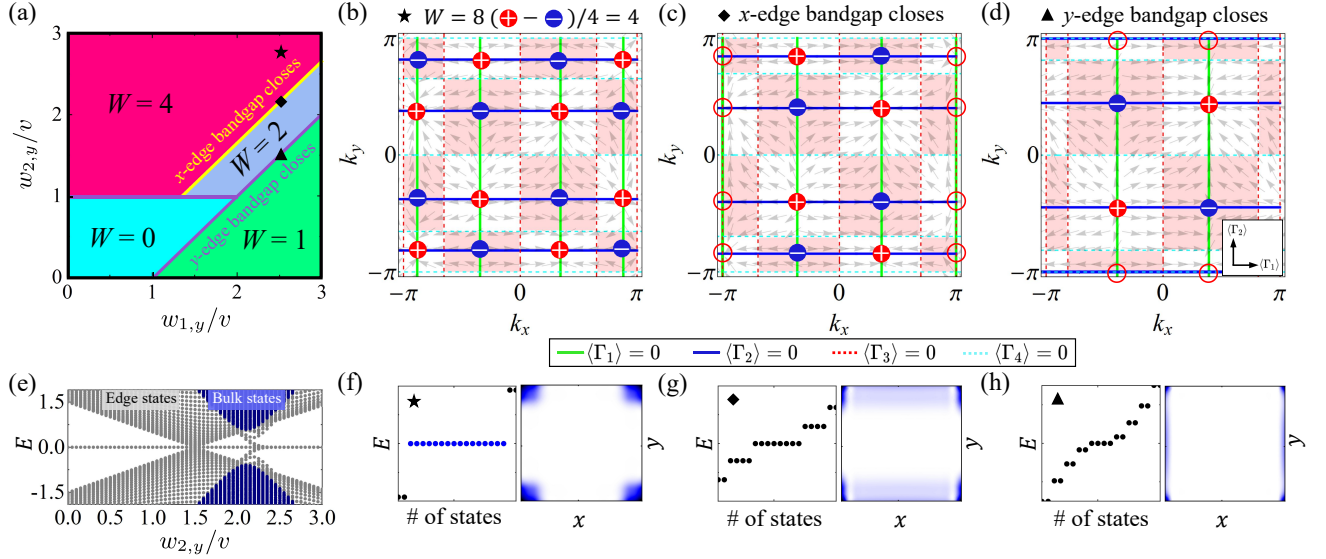


FIG. 2. (a) Phase diagram indicated by W . Pseudospin field $\Theta(\mathbf{k})$ with the marked topological charges \mathcal{C}_n and polarization $\mathcal{P}_n = +1$ in the white regions and -1 in the pink ones for (b) $W = 4$ when $w_{2,y} = 2.7v$ (star), and for (c) x - and (d) y -edge bandgap closing points when $w_{2,y} = 2.167v$ (rhombus) and $1.5v$ (triangle), respectively. Open red circles mark where the topological charges are annihilated or created. (e) Energy spectrum under the open-boundary condition in the different $w_{2,y}$ when $w_{1,y} = 2.5v$. The topological phase transitions occur at closing points of the edge-state band gap. (f)-(h) Zero-energy states and their real-space distributions for (b)-(d). We use $w_{1(2),x} = 3w_{1(2),y}$ and $w_{1,y} = 2.5v$.

realizable in quantum simulation experiments [81, 95, 96]. This provides an insightful picture to detect the chiral-symmetric HOTPs in the momentum space.

Next, we apply our theory to different classes of topological systems. We first consider a separable system whose topological phase transition occurs at the closing points of the edge-state band gap instead of the bulk one. It is an extended BBH model [67] with

$$\begin{aligned} h_{1(2)} &= v + w_{1,x(y)} \cos k_{x(y)} + w_{2,x(y)} \cos 2k_{x(y)}, \\ h_{3(4)} &= w_{1,x(y)} \sin k_{x(y)} + w_{2,x(y)} \sin 2k_{x(y)}. \end{aligned} \quad (5)$$

The Γ matrices are $\Gamma_1 = -\tau_x \sigma_z$, $\Gamma_2 = \tau_x \sigma_x$, $\Gamma_3 = -\tau_y$, and $\Gamma_4 = -\tau_x \sigma_y$. It has chiral symmetry under $\Gamma_5 = \tau_z$, mirror symmetry with $M_x = \tau_x$ and $M_y = \tau_y \sigma_y$, and inversion symmetry with $I = \tau_z \sigma_y$. The system belongs to the topological class AIII. We show in Fig. 2(a) the phase diagram described by W via studying the expectation values $\langle \Gamma_i(\mathbf{k}) \rangle$. It matches with the one described by the real-space MCNs [67]. When $w_{2,y} = 2.7v$, there are sixteen nodal points determined by $\Theta(\mathbf{k}) = 0$ [see Fig. 2(b)]. Their topological charges \mathcal{C}_n are identified by calculating the winding of $\Theta(\mathbf{k})$ around \mathbf{q}_n . The signs of $\langle \Gamma_{3,4}(\mathbf{q}_n) \rangle$ determine the polarizations, where $\mathcal{P}_n = +1$ and -1 are marked by the white and pink, respectively. We immediately have $W = 4$, which signifies that the system hosts sixteen degenerate zero-energy states localized at its corners [see Fig. 2(f)]. Figure 2(c) shows $\langle \Gamma_i(\mathbf{k}) \rangle$ and the polarizations at the phase boundary between $W = 4$ and 2 when $w_{2,y} = 2.167v$. Four pairs of nodal points satisfying $\langle \Gamma_{1,2}(\mathbf{q}_n) \rangle = 0$ merge to the line of $k_x = -\pi$ of

$\langle \Gamma_3(\mathbf{k}) \rangle = 0$, which, keeping the band gap of the bulk states open due to $\langle \Gamma_4(\mathbf{k}) \rangle \neq 0$, closes the band gap of x -edge states [see Figs. 2(e) and 2(g)]. It makes that the polarization of these nodal points vanish and a topological phase transition is triggered. A similar case of the phase boundary with a gap closing of the y -edge states is given in Figs. 2(d) and 2(h).

We further consider an inseparable system whose topological phase transition occurs at the closing point of the bulk-state band gap. Its h -components are

$$\begin{aligned} h_1 &= M - 2B[2 - \cos(pk_x) - \cos(pk_y)], \quad h_3 = \sin(pk_x), \\ h_2 &= \cos(2pk_x) - \cos(2pk_y), \quad h_4 = -\sin(pk_y), \end{aligned} \quad (6)$$

with an integer p . The Γ matrices are $\Gamma_1 = \sigma_z$, $\Gamma_2 = \tau_x \sigma_x$, $\Gamma_3 = \tau_z \sigma_x$, and $\Gamma_4 = \sigma_y$. The system has chiral symmetry under $\Gamma_5 = \tau_y \sigma_x$, time-reversal symmetry with $\mathcal{T} = \tau_x \mathcal{K}$, and particle-hole symmetry with $P = \tau_z \sigma_x \mathcal{K}$, where \mathcal{K} is complex conjugate operator. Therefore, it belongs to the class BDI. In addition to the symmetries of $M_x = \tau_y \sigma_z$, $M_y = \tau_x$, $I = \tau_z \sigma_z$, the system also has C_4 -rotation symmetry with $C_4 = \text{diag}(i, 1, -1, -i)$ and mirror-rotation symmetry with $M_{xy} = C_4 M_y$. The phase diagram characterized by W is shown in Fig. 3(a). The structures of $\Theta(\mathbf{k})$ when $(p, M/B) = (1, 2.0)$ figure out four nodal points, as shown in Fig. 3(b). Via calculating the winding of $\Theta(\mathbf{k})$ around \mathbf{q}_n , we have the topological charge \mathcal{C}_n of \mathbf{q}_n . Their polarization are achieved by examining the signs of $\langle \Gamma_{3,4}(\mathbf{q}_n) \rangle$. We then readily obtain $W = 1$, which signifies that four corner states are present. The energy spectrum under the open-boundary

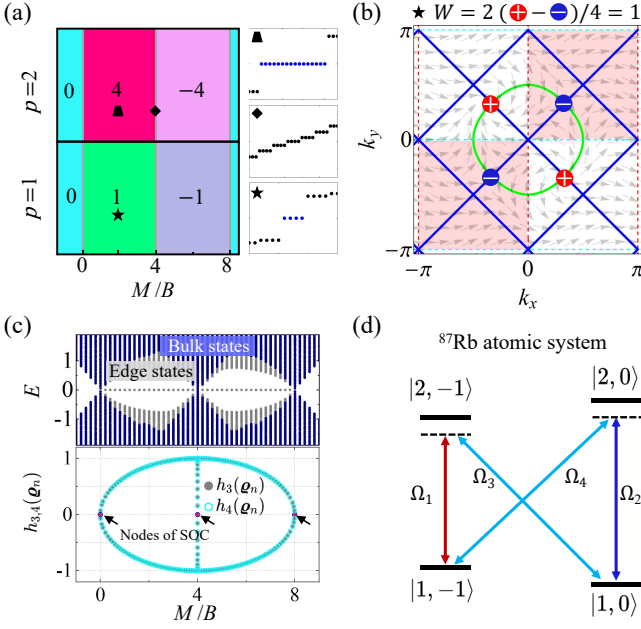


FIG. 3. (a) Phase diagrams indicated by W and zero-energy states when $(p, M/B) = (2, 2.0)$ (trapezoid), $(2, 4.0)$ (rhombus), and $(1, 2.0)$ (star). (b) Pseudospin structures of $\Theta(\mathbf{k})$ with the marked \mathcal{C}_n and polarization for $W = 1$ when $(p, M/B) = (1, 2.0)$. (c) Energy spectrum under the open-boundary conditions (upper). The numerical results of $h_{3,4}(\mathbf{q}_n)$ (lower), where $h_{3,4}(\mathbf{q}_n) = 0$ (red solid points and blue open cycles) emerging at $M = 0, 4B$, and $8B$ gives the topological phase transitions driven by bulk-state band gap closing. (d) Simulation of the Hamiltonian of class BDI by a four-level atomic system.

condition in Fig. 3(c) reveals that the phase transition occurs at the closing points of the band gap of the bulk states. Such a phase transition is caused by the vanishing of the charge polarizations \mathcal{P}_n driven by $h_{3,4}(\mathbf{q}_n) = 0$.

Besides, keeping h -components as Eq. (6) but changing the Γ matrices as $\Gamma_1 = \tau_x$, $\Gamma_2 = \rho_z \tau_z \sigma_x$, $\Gamma_3 = \rho_z \tau_y$, $\Gamma_4 = \rho_z \tau_z \sigma_y$, and $\Gamma_5 = \rho_z \tau_z \sigma_z$, we shall obtain a second-order topological phase belonging to class CII, where $2W$ gives the second-order topology of the corner states and we can identify W like the BDI case.

Experimental scheme.—Based on the realization of Bernevig-Hughes-Zhang (BHZ) model in the recent experiment [84], we provide a scheme to realize the 2D chiral-symmetric second-order topological phases in ^{87}Rb cold atomic system. We take $p = 1$ as an example to demonstrate our scheme. By employing four atomic hyperfine levels $|a\rangle = |2, -1\rangle$, $|b\rangle = |1, -1\rangle$, $|c\rangle = |2, 0\rangle$, and $|d\rangle = |1, 0\rangle$, we apply four microwaves to couple $\{|a\rangle, |b\rangle\}$, $\{|c\rangle, |d\rangle\}$, $\{|a\rangle, |d\rangle\}$, and $\{|c\rangle, |b\rangle\}$ with Rabi frequencies $\Omega_1 = -\Omega_2 = (h_3^2 + h_4^2)^{1/2}$ and $\Omega_3 = \Omega_4 = h_2$ and phases $\varphi_1 = -\varphi_2 = \arctan(h_4/h_3)$ and $\varphi_3 = \varphi_4 = 0$ [see Fig. 3(c)]. Then, Eq. (6) is obtained on the bare-state basis $\{|a\rangle, |b\rangle, |c\rangle, |d\rangle\}$ [93]. It is found that the \mathbf{k} -dependent h_2 term opens band gap of the helical states of

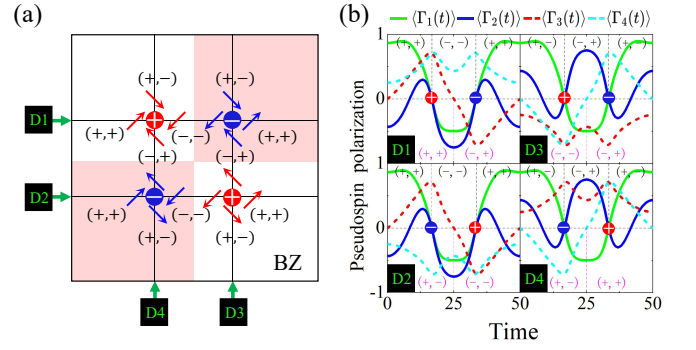


FIG. 4. (a) Detecting polarized topological charges by sweeping $k_{x(y)}$ at four lines $D_{1,2,3,4}$ of BZ. (b) Dynamical pseudospin polarizations $\langle \Gamma_i(t) \rangle$ of $p = 1$, where $\langle \Gamma_{1,2}(t) \rangle = 0$ give the locations of the nodal points. Signs of $\langle \Gamma_{1,2}(t) \rangle$ and $\langle \Gamma_{3,4}(t) \rangle$ near at the nodal points are marked by black and pink, determining their charges and polarizations, respectively.

the BHZ model and induces the corner states, rendering a second-order topological phases.

The topological charges and their charge polarizations can be detected by the following dynamical way [84]. Choosing one fixed $k_{y(x)}$ and sweeping $k_{x(y)}$ at a rate $v_{k_{x(y)}} = 2\pi/T$, i.e., $k_{x(y)}(t) = v_{k_{x(y)}}t - \pi$ with $t \in [0, T]$, we perform the measurements along four different momentum lines $D_{1,2,3,4}$ of BZ, which covers all the topological charges [see Fig. 4(a)]. It is seen that the nodal points are captured by the dynamical expectation values $\langle \Gamma_1(t) \rangle = \langle \Gamma_2(t) \rangle = 0$ [see Fig. 4(b)]. The topological charges and charge polarizations are determined by the signs of $\langle \Gamma_{1,2}(t) \rangle$ and $\langle \Gamma_{3,4}(t) \rangle$ near at these nodal points, respectively [see Figs. 4(a) and 4(b)]. We can finally identify $W = 1$ in this second-order topological system. These results provide possibility to observe the chiral-symmetric HOTPs in quantum simulations.

The dD generalization.—Our characterization can be generalized to describe the d th-order topological phases in dD chiral-symmetric systems. We consider a dD topological system described by $\mathcal{H}(\mathbf{k}) = \sum_{i=1}^{2d} h_i(\mathbf{k})\Gamma_i$. In a similar manner to the 2D case, we separate $\mathbf{h}(\mathbf{k}) = (\mathbf{h}_m, \mathbf{h}_{so})$, with $\mathbf{h}_m = (h_1, \dots, h_d)$ and $\mathbf{h}_{so} = (h_{d+1}, \dots, h_{2d})$. Its d th-order topology is well characterized by the topological invariant [93]

$$W = \frac{1}{(-2)^d} \sum_n \mathcal{C}_n \mathcal{P}_n, \quad (7)$$

where $\mathcal{C}_n = \text{sgn}\{\det[\partial h_{m,i}(\mathbf{q}_n)/\partial k_j]\}$ are the topological charges located at the nodal points \mathbf{q}_n and determined by $\mathbf{h}_m(\mathbf{q}_n) = 0$. The charge polarizations reads $\mathcal{P}_n = \text{sgn}[h_{d+1}(\mathbf{q}_n) \cdots h_{2d}(\mathbf{q}_n)]$. Accordingly, the different types of d th-order topological phase transitions are captured by the emergence or merger of topological charges in the zero polarization regions. This theory opens an avenue for characterizing the chiral-symmetric HOTPs in the momentum space.

Discussion and Conclusion.—Although only the Hermitian and static systems are considered, our theory may also have broad implications in characterizing the HOTPs of the Floquet and non-Hermitian systems. After introducing the longer-range hopping into BBH model and further adding the periodic driving or non-Hermitian term, the topological invariants in Refs. [54] and [58] cannot characterize these topological states anymore. Generalizing the real-space topological invariants [67–69] in these systems also becomes exceptionally difficult. Nevertheless, the polarized topological charges may provide an insight to solve these interesting questions [97].

In summary, we have proposed a momentum-space topological characterization to chiral-symmetric HOTPs via the polarized topological charges. After separating the momentum-space Hamiltonian into the dispersion and pseudospin-orbit coupling terms, we can identify all the nodal points and their topological charges from the dispersion terms. The pseudospin-orbit coupling term opens the band gap and causes the polarizations of all topological charges. The HOTPs are characterized by the total polarized topological charges. This theory also inspires a feasible experimental detection to the HOTPs in the ^{87}Rb atomic system. Providing an elegant way to characterize \mathbb{Z} -classified HOTPs and hopefully can be extended to \mathbb{Z}_2 -classified ones, it prompts the development of higher-order topological classification theory.

Acknowledgements. The work is supported by the National Natural Science Foundation (Grants No. 12275109 and No. 12247101).

* anjhong@lzu.edu.cn

- [1] W. A. Benalcazar, B. A. Bernevig, and T. L. Hughes, Quantized electric multipole insulators, *Science* **357**, 61 (2017).
- [2] J. Langbehn, Y. Peng, L. Trifunovic, F. von Oppen, and P. W. Brouwer, Reflection-symmetric second-order topological insulators and superconductors, *Phys. Rev. Lett.* **119**, 246401 (2017).
- [3] Z. Song, Z. Fang, and C. Fang, (d-2)-dimensional edge states of rotation symmetry protected topological states, *Phys. Rev. Lett.* **119**, 246402 (2017).
- [4] W. A. Benalcazar, B. A. Bernevig, and T. L. Hughes, Electric multipole moments, topological multipole moment pumping, and chiral hinge states in crystalline insulators, *Phys. Rev. B* **96**, 245115 (2017).
- [5] E. Khalaf, Higher-order topological insulators and superconductors protected by inversion symmetry, *Phys. Rev. B* **97**, 205136 (2018).
- [6] M. Ezawa, Higher-order topological insulators and semimetals on the breathing kagome and pyrochlore lattices, *Phys. Rev. Lett.* **120**, 026801 (2018).
- [7] F. Schindler, A. M. Cook, M. G. Vergniory, Z. Wang, S. S. Parkin, B. A. Bernevig, and T. Neupert, Higher-order topological insulators, *Sci. Adv.* **4**, eaat0346 (2018).
- [8] E. Khalaf, H. C. Po, A. Vishwanath, and H. Watanabe, Symmetry indicators and anomalous surface states of topological crystalline insulators, *Phys. Rev. X* **8**, 031070 (2018).
- [9] S. A. A. Ghorashi, T. L. Hughes, and E. Rossi, Vortex and surface phase transitions in superconducting higher-order topological insulators, *Phys. Rev. Lett.* **125**, 037001 (2020).
- [10] M. Kheirkhah, Z. Yan, Y. Nagai, and F. Marsiglio, First- and second-order topological superconductivity and temperature-driven topological phase transitions in the extended hubbard model with spin-orbit coupling, *Phys. Rev. Lett.* **125**, 017001 (2020).
- [11] C.-A. Li, B. Fu, Z.-A. Hu, J. Li, and S.-Q. Shen, Topological phase transitions in disordered electric quadrupole insulators, *Phys. Rev. Lett.* **125**, 166801 (2020).
- [12] X. Wu, W. A. Benalcazar, Y. Li, R. Thomale, C.-X. Liu, and J. Hu, Boundary-obstructed topological high- T_c superconductivity in iron pnictides, *Phys. Rev. X* **10**, 041014 (2020).
- [13] M. Ezawa, Edge-corner correspondence: Boundary-obstructed topological phases with chiral symmetry, *Phys. Rev. B* **102**, 121405(R) (2020).
- [14] K. Asaga and T. Fukui, Boundary-obstructed topological phases of a massive Dirac fermion in a magnetic field, *Phys. Rev. B* **102**, 155102 (2020).
- [15] J. Claes and T. L. Hughes, Wannier band transitions in disordered π -flux ladders, *Phys. Rev. B* **102**, 100203(R) (2020).
- [16] L. Li, W. Zhu, and J. Gong, Direct dynamical characterization of higher-order topological phases with nested band inversion surfaces, *Sci. Bull.* **66**, 1502 (2021).
- [17] E. Khalaf, W. A. Benalcazar, T. L. Hughes, and R. Queiroz, Boundary-obstructed topological phases, *Phys. Rev. Research* **3**, 013239 (2021).
- [18] Y.-B. Yang, K. Li, L.-M. Duan, and Y. Xu, Type-II quadrupole topological insulators, *Phys. Rev. Research* **2**, 033029 (2020).
- [19] N. Mao, R. Li, Y. Dai, B. Huang, B. Yan, and C. Niu, Orbital Shift-Induced Boundary Obstructed Topological Materials with a Large Energy Gap, *Adv. Sci.* **20**, 2202564 (2022).
- [20] J.-H. Chen, Z.-Z. Yang, W.-J. Yang, A.-Y. Guan, X.-Y. Zou, and J.-C. Cheng, Experimental realization of boundary-obstructed topological insulators using acoustic two-dimensional Su–Schrieffer–Heeger network, *Appl. Phys. Lett.* **120**, 253508 (2022).
- [21] Y.-B. Yang, J.-H. Wang, K. Li, and Y. Xu, Higher-order topological phases in crystalline and non-crystalline systems: a review, *J. Phys. Condens. Matter* (2024).
- [22] S.-B. Zhang, W. Rui, A. Calzona, S.-J. Choi, A. P. Schnyder, and B. Trauzettel, Topological and holonomic quantum computation based on second-order topological superconductors, *Phys. Rev. Research* **2**, 043025 (2020).
- [23] C.-A. Li, S.-B. Zhang, J. Li, and B. Trauzettel, Higher-order Fabry–Pérot interferometer from topological hinge states, *Phys. Rev. Lett.* **127**, 026803 (2021).
- [24] L. Trifunovic and P. W. Brouwer, Higher-order bulk-boundary correspondence for topological crystalline phases, *Phys. Rev. X* **9**, 011012 (2019).
- [25] R. Queiroz and A. Stern, Splitting the hinge mode of higher-order topological insulators, *Phys. Rev. Lett.* **123**, 036802 (2019).
- [26] M. J. Park, Y. Kim, G. Y. Cho, and S. B. Lee, Higher-order topological insulator in twisted bilayer graphene,

- Phys. Rev. Lett. **123**, 216803 (2019).
- [27] X.-L. Sheng, C. Chen, H. Liu, Z. Chen, Z.-M. Yu, Y. X. Zhao, and S. A. Yang, Two-dimensional second-order topological insulator in graphdiyne, *Phys. Rev. Lett.* **123**, 256402 (2019).
 - [28] D. Călugăru, V. Juričić, and B. Roy, Higher-order topological phases: A general principle of construction, *Phys. Rev. B* **99**, 041301(R) (2019).
 - [29] A. Tiwari, M.-H. Li, B. A. Bernevig, T. Neupert, and S. A. Parameswaran, Unhinging the Surfaces of Higher-Order Topological Insulators and Superconductors, *Phys. Rev. Lett.* **124**, 046801 (2020).
 - [30] R.-X. Zhang, F. Wu, and S. DasSarma, Möbius insulator and higher-order topology in $\text{MnBi}_{2n}\text{Te}_{3n+1}$, *Phys. Rev. Lett.* **124**, 136407 (2020).
 - [31] R. Chen, C.-Z. Chen, J.-H. Gao, B. Zhou, and D.-H. Xu, Higher-order topological insulators in quasicrystals, *Phys. Rev. Lett.* **124**, 036803 (2020).
 - [32] R. Noguchi, M. Kobayashi, Z. Jiang, K. Kuroda, T. Takahashi, Z. Xu, D. Lee, M. Hirayama, M. Ochi, T. Shira-sawa, *et al.*, Evidence for a higher-order topological insulator in a three-dimensional material built from van der Waals stacking of bismuth-halide chains, *Nat. Mater.* **20**, 473 (2021).
 - [33] Q. Wei, X. Zhang, W. Deng, J. Lu, X. Huang, M. Yan, G. Chen, Z. Liu, and S. Jia, 3D hinge transport in acoustic higher-order topological insulators, *Phys. Rev. Lett.* **127**, 255501 (2021).
 - [34] J. Du, T. Li, X. Fan, Q. Zhang, and C. Qiu, Acoustic realization of surface-obstructed topological insulators, *Phys. Rev. Lett.* **128**, 224301 (2022).
 - [35] W. Jia, X.-C. Zhou, L. Zhang, L. Zhang, and X.-J. Liu, Unified characterization for higher-order topological phase transitions, *Phys. Rev. Research* **5**, L022032 (2023).
 - [36] M. Lin and T. L. Hughes, Topological quadrupolar semimetals, *Phys. Rev. B* **98**, 241103 (2018).
 - [37] J. Ahn, D. Kim, Y. Kim, and B.-J. Yang, Band topology and linking structure of nodal line semimetals with Z_2 monopole charges, *Phys. Rev. Lett.* **121**, 106403 (2018).
 - [38] Z. Wang, B. J. Wieder, J. Li, B. Yan, and B. A. Bernevig, Higher-Order Topology, Monopole Nodal Lines, and the Origin of Large Fermi Arcs in Transition Metal Dichalcogenides X Te_2 ($\text{X} = \text{Mo}, \text{W}$), *Phys. Rev. Lett.* **123**, 186401 (2019).
 - [39] Y. Xu, L. Elcoro, Z.-D. Song, B. J. Wieder, M. Vergniory, N. Regnault, Y. Chen, C. Felser, and B. A. Bernevig, High-throughput calculations of magnetic topological materials, *Nature* **586**, 702 (2020).
 - [40] H.-X. Wang, Z.-K. Lin, B. Jiang, G.-Y. Guo, and J.-H. Jiang, Higher-order Weyl semimetals, *Phys. Rev. Lett.* **125**, 146401 (2020).
 - [41] S. A. A. Ghorashi, T. Li, and T. L. Hughes, Higher-order Weyl semimetals, *Phys. Rev. Lett.* **125**, 266804 (2020).
 - [42] T. Liu, J. J. He, Z. Yang, and F. Nori, Higher-order Weyl-exceptional-ring semimetals, *Phys. Rev. Lett.* **127**, 196801 (2021).
 - [43] Z. Pu, H. He, L. Luo, Q. Ma, L. Ye, M. Ke, and Z. Liu, Acoustic Higher-Order Weyl Semimetal with Bound Hinge States in the Continuum, *Phys. Rev. Lett.* **130**, 116103 (2023).
 - [44] Z. Yan, F. Song, and Z. Wang, Majorana corner modes in a high-temperature platform, *Phys. Rev. Lett.* **121**, 096803 (2018).
 - [45] C.-H. Hsu, P. Stano, J. Klinovaja, and D. Loss, Majorana Kramers pairs in higher-order topological insulators, *Phys. Rev. Lett.* **121**, 196801 (2018).
 - [46] Z. Yan, Higher-order topological odd-parity superconductors, *Phys. Rev. Lett.* **123**, 177001 (2019).
 - [47] X. Zhu, Second-order topological superconductors with mixed pairing, *Phys. Rev. Lett.* **122**, 236401 (2019).
 - [48] Y. Volpez, D. Loss, and J. Klinovaja, Second-order topological superconductivity in π -junction Rashba layers, *Phys. Rev. Lett.* **122**, 126402 (2019).
 - [49] F. Schindler, B. Bradlyn, M. H. Fischer, and T. Neupert, Pairing obstructions in topological superconductors, *Phys. Rev. Lett.* **124**, 247001 (2020).
 - [50] Y. Tan, Z.-H. Huang, and X.-J. Liu, Two-particle Berry phase mechanism for Dirac and Majorana Kramers pairs of corner modes, *Phys. Rev. B* **105**, L041105 (2022).
 - [51] A. Chew, Y. Wang, B. A. Bernevig, and Z.-D. Song, Higher-order topological superconductivity in twisted bilayer graphene, *Phys. Rev. B* **107**, 094512 (2023).
 - [52] Y. Peng and G. Refael, Floquet second-order topological insulators from nonsymmorphic space-time symmetries, *Phys. Rev. Lett.* **123**, 016806 (2019).
 - [53] B. Huang and W. V. Liu, Floquet higher-order topological insulators with anomalous dynamical polarization, *Phys. Rev. Lett.* **124**, 216601 (2020).
 - [54] H. Hu, B. Huang, E. Zhao, and W. V. Liu, Dynamical singularities of Floquet higher-order topological insulators, *Phys. Rev. Lett.* **124**, 057001 (2020).
 - [55] X.-W. Luo and C. Zhang, Higher-order topological corner states induced by gain and loss, *Phys. Rev. Lett.* **123**, 073601 (2019).
 - [56] C. H. Lee, L. Li, and J. Gong, Hybrid higher-order skin-topological modes in nonreciprocal systems, *Phys. Rev. Lett.* **123**, 016805 (2019).
 - [57] Z. Zhang, M. R. López, Y. Cheng, X. Liu, and J. Christensen, Non-Hermitian sonic second-order topological insulator, *Phys. Rev. Lett.* **122**, 195501 (2019).
 - [58] T. Liu, Y.-R. Zhang, Q. Ai, Z. Gong, K. Kawabata, M. Ueda, and F. Nori, Second-order topological phases in non-Hermitian systems, *Phys. Rev. Lett.* **122**, 076801 (2019).
 - [59] A. A. Stepanenko, M. D. Lyubarov, and M. A. Gorlach, Higher-order topological phase of interacting photon pairs, *Phys. Rev. Lett.* **128**, 213903 (2022).
 - [60] J. May-Mann, Y. You, T. L. Hughes, and Z. Bi, Interaction Enabled Fractonic Higher-Order Topological Phases, *Phys. Rev. B* **105**, 245122 (2022).
 - [61] Z. Yang, E. Lustig, Y. Lumer, and M. Segev, Photonic floquet topological insulators in a fractal lattice, *Light: Sci. & Appl.* **9**, 1 (2020).
 - [62] S. Zheng, X. Man, Z.-L. Kong, Z.-K. Lin, G. Duan, N. Chen, D. Yu, J.-H. Jiang, and B. Xia, Observation of fractal higher-order topological states in acoustic metamaterials, *Sci. Bull.* **67**, 2069 (2022).
 - [63] A. Altland and M. R. Zirnbauer, Nonstandard symmetry classes in mesoscopic normal-superconducting hybrid structures, *Phys. Rev. B* **55**, 1142 (1997).
 - [64] A. Kitaev, Periodic table for topological insulators and superconductors, *AIP Conf. Proc.* **1134**, 22 (2009).
 - [65] S. Ryu, A. P. Schnyder, A. Furusaki, and A. W. Ludwig, Topological insulators and superconductors: tenfold way and dimensional hierarchy, *New J. Phys.* **12**, 065010 (2010).
 - [66] C.-K. Chiu, J. C. Teo, A. P. Schnyder, and S. Ryu, Classi-

- fication of topological quantum matter with symmetries, *Rev. Mod. Phys.* **88**, 035005 (2016).
- [67] W. A. Benalcazar and A. Cerjan, Chiral-Symmetric Higher-Order Topological Phases of Matter, *Phys. Rev. Lett.* **128**, 127601 (2022).
- [68] L. Lin and C. Lee, Probing chiral-symmetric higher-order topological insulators with multipole winding number, *arXiv:2401.03699* (2024).
- [69] J.-Z. Li, X.-J. Luo, F. Wu, and M. Xiao, Exact universal characterization of chiral-symmetric higher-order topological phases, *arXiv:2404.19757* (2024).
- [70] D. Wang, Y. Deng, M. Oudich, W. A. Benalcazar, G. Ma, and Y. Jing, Realization of a Z-Classified Chiral-Symmetric Higher-Order Topological Insulator in a Coupling-Inverted Acoustic Crystal, *Phys. Rev. Lett.* **131**, 157201 (2023).
- [71] Y. Li, H. Qiu, Q. Zhang, and C. Qiu, Acoustic higher-order topological insulators protected by multipole chiral numbers, *Phys. Rev. B* **108**, 205135 (2023).
- [72] Y. Li, J.-H. Zhang, F. Mei, B. Xie, M.-H. Lu, J. Ma, L. Xiao, and S. Jia, Large-chiral-number corner modes in Z-class higher-order topoelectrical circuits, *Phys. Rev. Applied* **20**, 064042 (2023).
- [73] M. Z. Hasan and C. L. Kane, Colloquium: topological insulators, *Rev. Mod. Phys.* **82**, 3045 (2010).
- [74] X.-L. Qi and S.-C. Zhang, Topological insulators and superconductors, *Rev. Mod. Phys.* **83**, 1057 (2011).
- [75] I. Bloch, J. Dalibard, and S. Nascimbene, Quantum simulations with ultracold quantum gases, *Nat. Phys.* **8**, 267 (2012).
- [76] G. Jotzu, M. Messer, R. Desbuquois, M. Lebrat, T. Uehlinger, D. Greif, and T. Esslinger, Experimental realization of the topological Haldane model with ultracold fermions, *Nature* **515**, 237 (2014).
- [77] Z. Wu, L. Zhang, W. Sun, X.-T. Xu, B.-Z. Wang, S.-C. Ji, Y. Deng, S. Chen, X.-J. Liu, and J.-W. Pan, Realization of two-dimensional spin-orbit coupling for Bose-Einstein condensates, *Science* **354**, 83 (2016).
- [78] F. Schäfer, T. Fukuhara, S. Sugawa, Y. Takasu, and Y. Takahashi, Tools for quantum simulation with ultracold atoms in optical lattices, *Nat. Rev. Phys.* **2**, 411 (2020).
- [79] F. Kong, C. Ju, Y. Liu, C. Lei, M. Wang, X. Kong, P. Wang, P. Huang, Z. Li, F. Shi, *et al.*, Direct measurement of topological numbers with spins in diamond, *Phys. Rev. Lett.* **117**, 060503 (2016).
- [80] A. Ariyaratne, D. Bluvstein, B. A. Myers, and A. C. B. Jayich, Nanoscale electrical conductivity imaging using a nitrogen-vacancy center in diamond, *Nat. Commun.* **9**, 1 (2018).
- [81] W. Ji, L. Zhang, M. Wang, L. Zhang, Y. Guo, Z. Chai, X. Rong, F. Shi, X.-J. Liu, Y. Wang, and J. Du, Quantum simulation for three-dimensional chiral topological insulator, *Phys. Rev. Lett.* **125**, 020504 (2020).
- [82] T. Xin, Y. Li, Y.-a. Fan, X. Zhu, Y. Zhang, X. Nie, J. Li, Q. Liu, and D. Lu, Quantum Phases of Three-Dimensional Chiral Topological Insulators on a Spin Quantum Simulator, *Phys. Rev. Lett.* **125**, 090502 (2020).
- [83] D. Zhao, C. Wei, S. Xue, Y. Huang, X. Nie, J. Li, D. Ruan, D. Lu, T. Xin, and G. Long, Characterizing quantum simulations with quantum tomography on a spin quantum simulator, *Phys. Rev. A* **103**, 052403 (2021).
- [84] Q.-X. Lv, Y.-X. Du, Z.-T. Liang, H.-Z. Liu, J.-H. Liang, L.-Q. Chen, L.-M. Zhou, S.-C. Zhang, D.-W. Zhang, B.-Q. Ai, *et al.*, Measurement of spin Chern numbers in quantum simulated topological insulators, *Phys. Rev. Lett.* **127**, 136802 (2021).
- [85] Z. Lei, Y. Deng, and L. Li, Topological classification of higher-order topological phases with nested band inversion surfaces, *Phys. Rev. B* **106**, 245105 (2022).
- [86] X.-J. Luo, X.-H. Pan, C.-X. Liu, and X. Liu, Higher-order topological phases emerging from Su-Schrieffer-Heeger stacking, *Phys. Rev. B* **107**, 045118 (2023).
- [87] T. Morimoto and A. Furusaki, Topological classification with additional symmetries from Clifford algebras, *Phys. Rev. B* **88**, 125129 (2013).
- [88] C.-K. Chiu, H. Yao, and S. Ryu, Classification of topological insulators and superconductors in the presence of reflection symmetry, *Phys. Rev. B* **88**, 075142 (2013).
- [89] D. Sticlet, F. Piéchon, J.-N. Fuchs, P. Kalugin, and P. Simon, Geometrical engineering of a two-band chern insulator in two dimensions with arbitrary topological index, *Phys. Rev. B* **85**, 165456 (2012).
- [90] L. Zhang, L. Zhang, S. Niu, and X.-J. Liu, Dynamical classification of topological quantum phases, *Sci. Bull.* **63**, 1385 (2018).
- [91] L. Zhang, L. Zhang, and X.-J. Liu, Dynamical detection of topological charges, *Phys. Rev. A* **99**, 053606 (2019).
- [92] W. Jia, L. Zhang, L. Zhang, and X.-J. Liu, Dynamically characterizing topological phases by high-order topological charges, *Phys. Rev. A* **103**, 052213 (2021).
- [93] See Supplemental Material for the detailed analysis of the polarized topological charges in first- and higher-order topological systems, the numerical results for 2D second-order and 3D third-order topological phases, and the experimental scheme in ^{87}Rb atomic system to realize the chiral-symmetric second-order topological phases.
- [94] R. Okugawa, S. Hayashi, and T. Nakanishi, Second-order topological phases protected by chiral symmetry, *Phys. Rev. B* **100**, 235302 (2019).
- [95] X.-L. Yu, W. Ji, L. Zhang, Y. Wang, J. Wu, and X.-J. Liu, Quantum dynamical characterization and simulation of topological phases with high-order band inversion surfaces, *Phys. Rev. X Quantum* **2**, 020320 (2021).
- [96] J. Niu, T. Yan, Y. Zhou, Z. Tao, X. Li, W. Liu, L. Zhang, H. Jia, S. Liu, Z. Yan, Y. Chen, and D. Yu, Simulation of higher-order topological phases and related topological phase transitions in a superconducting qubit, *Sci. Bull.* **66**, 1168 (2021).
- [97] L. Zhang, L. Zhang, and X.-J. Liu, Unified theory to characterize Floquet topological phases by quench dynamics, *Phys. Rev. Lett.* **125**, 183001 (2020).

Supplementary Material for “Unveiling Higher-Order Topology via Polarized Topological Charges”

Wei Jia,¹ Bao-Zong Wang,² Ming-Jian Gao,¹ and Jun-Hong An^{1,*}

¹Key Laboratory of Quantum Theory and Applications of MoE, Lanzhou Center for Theoretical Physics, and Key Laboratory of Theoretical Physics of Gansu Province, Lanzhou University, Lanzhou 730000, China

²International Center for Quantum Materials, School of Physics, Peking University, Beijing 100871, China

In this Supplementary Material, we provide the details of polarized topological charge in first-order and higher-order topological systems in Secs. I and II, respectively. We also show the numerical results for second-order and third-order topological phases with chiral symmetry in Sec. III. We further give the higher-order topological phase transitions determined by the polarized topological charges in Sec. IV. We finally provide the experimental scheme in ⁸⁷Rb atomic system to realize the chiral-symmetric topological phase with corner states in Sec. V.

I. POLARIZED TOPOLOGICAL CHARGES IN FIRST-ORDER TOPOLOGICAL SYSTEMS

We first propose the concept of polarized topological charge in the first-order topological systems. Our starting point is a one-dimensional (1D) chiral-symmetric topological phases in the \mathbb{Z} topological classification, such as a Su–Schrieffer–Heeger (SSH) model along x direction. The corresponding momentum-space Hamiltonian is written as

$$\mathcal{H}(k_x) = h_1(k_x)\tau_x + h_3(k_x)\tau_y, \quad (\text{S1})$$

where $\tau_{x,y,z}$ are Pauli matrices. This system has chiral symmetry $\tau_z\mathcal{H}(k_x)\tau_z = \mathcal{H}(-k_x)$ under the chiral operator τ_z . Thus, its first-order topology is characterized by the winding number

$$W_x = \frac{1}{2\pi i} \int_{\text{BZ}} \text{Tr} [q(k_x)^\dagger \partial_{k_x} q(k_x)], \quad (\text{S2})$$

where q is a unitary matrix and defines a map from the 1D Brillouin zone (BZ) to the space of unitary matrices $U(n)$. This gives an integer topological classification by the first homotopy group, i.e., $\pi_1[U(n)] = \mathbb{Z}$. Hence W_x is an integer topological invariant to describe the first-order topological phase with chiral symmetry. Remarkably, W_x can also be determined by the characterization scheme with polarized topological charges. We use the convention that $h_1(k_x)$ denotes the band dispersion, while $h_3(k_x)$ denotes the pseudospin-orbit (SO) coupling. N_x nodal points are found from the band dispersion $h_1(\varrho_l) = 0$. We can define a topological charge to each ϱ_l as

$$\mathcal{C}_l^x = \text{sgn} \left[\frac{\partial h_1(\varrho_l)}{\partial k_x} \right]. \quad (\text{S3})$$

The presence of the pseudospin-orbit coupling term opens the band gap and make the topological charge \mathcal{C}_l polarized in an amount

$$\mathcal{P}_l^x = \text{sgn} [h_3(\varrho_l)]. \quad (\text{S4})$$

Then, one can analytically prove that Eq. (S2) is equivalent to

$$W_x = -\frac{1}{2} \sum_{l=1}^{N_x} \mathcal{C}_l^x \mathcal{P}_l^x, \quad (\text{S5})$$

where $\mathcal{C}_l^x \mathcal{P}_l^x$ is called a polarized topological charge. It should be noted that we hereby use the properties of all the polarized topological charges in the BZ to characterize W_x . Physically, each \mathcal{C}_l^x is defined on a nodal point of the band dispersion, and then the nonzero SO coupling opens energy gap at this nodal point, which makes \mathcal{C}_l^x obtain a nonzero polarization \mathcal{P}_l^x . This tells us that all the polarized topological charges of the BZ are nonzero for a gapped topological phase, while the emergence of one zero-value polarized topological charge can drive the topological phase transition, where the energy band gap is closing at this nodal point.

* anjhong@lzu.edu.cn

II. POLARIZED TOPOLOGICAL CHARGES IN HIGHER-ORDER TOPOLOGICAL SYSTEMS

A. Special 2D separable systems

Next we shall generalize the concept of polarized topological charge to higher-order topological systems. We first consider the special 2D lattice systems hosting second-order topological phases within the \mathbb{Z} classification, such as Benalcazar-Bernevig-Hughes (BBH) model [1] or 2D SSH model [2], which can be obtained by stacking y -directional SSH along x direction. Its momentum-space Hamiltonian is written as

$$\mathcal{H}(k_x, k_y) = h_1(k_x)\Gamma_1 + h_2(k_y)\Gamma_2 + h_3(k_x)\Gamma_3 + h_4(k_y)\Gamma_4. \quad (\text{S6})$$

This Hamiltonian can be translated to a separable form $\mathcal{H}(k_x, k_y) = \mathcal{H}(k_x) \otimes 1 + \tau_z \otimes \mathcal{H}(k_y)$ for a BBH model or $\mathcal{H}(k_x, k_y) = \mathcal{H}(k_x) \otimes \sigma_y + 1 \otimes \mathcal{H}(k_y)$ for a 2D SSH model. Due to separability of k_x and k_y in Eq. (S6), its second-order topology can be characterized by $W = W_x W_y$ [3]. Then, from Eq. (S5) and the similar form of W_y , we have

$$W = \frac{1}{4} \sum_{l=1}^{N_x} \mathcal{C}_l^x \mathcal{P}_l^x \sum_{m=1}^{N_y} \mathcal{C}_m^y \mathcal{P}_m^y. \quad (\text{S7})$$

Redefining the topological charges for the $N_x N_y$ nodal points (ϱ_l, ϱ_m) as

$$\mathcal{C}_n = \mathcal{C}_l^x \mathcal{C}_m^y = \text{sgn} \begin{bmatrix} \partial_{k_x} h_1(\varrho_l) & 0 \\ 0 & \partial_{k_y} h_2(\varrho_m) \end{bmatrix}, \quad (\text{S8})$$

and the corresponding polarizations as $\mathcal{P}_n = \mathcal{P}_l^x \mathcal{P}_m^y = \text{sgn}[h_3(\varrho_l)h_4(\varrho_m)]$, Eq. (S7) is recast into

$$\begin{aligned} W &= \frac{1}{4} (\mathcal{C}_1^x \mathcal{C}_1^y \mathcal{P}_1^x \mathcal{P}_1^y + \mathcal{C}_1^x \mathcal{C}_2^y \mathcal{P}_1^x \mathcal{P}_2^y \cdots + \mathcal{C}_{N_x}^x \mathcal{C}_{N_y}^y \mathcal{P}_{N_x}^x \mathcal{P}_{N_y}^y) \\ &= \frac{1}{4} (\mathcal{C}_1 \mathcal{P}_1 + \mathcal{C}_2 \mathcal{P}_2 \cdots + \mathcal{C}_{N_x \times N_y} \mathcal{P}_{N_x \times N_y}) \\ &= \frac{1}{4} \sum_{n=1}^{N_x \times N_y} \mathcal{C}_n \mathcal{P}_n. \end{aligned} \quad (\text{S9})$$

Thus, the special 2D separable system is well described by the polarized topological charges.

B. Generic 2D separable systems

Next we generalize the polarized topological charges to the generic 2D separable systems, in which we use a key idea that the generic separable Hamiltonian can be deformed to the special separable Hamiltonian without changing topology [4]. To demonstrate this point, we start from the following Hamiltonian

$$\mathcal{H}(k_x, k_y) = \frac{g_1(k_x) - g_2(k_y)}{\sqrt{2}} \Gamma_1 + \frac{g_1(k_x) + g_2(k_y)}{\sqrt{2}} \Gamma_2 + \frac{g_3(k_x) - g_4(k_y)}{\sqrt{2}} \Gamma_3 + \frac{g_3(k_x) + g_4(k_y)}{\sqrt{2}} \Gamma_4, \quad (\text{S10})$$

which is obviously not a special separable Hamiltonian as Eq. (S6). By taking $\tilde{\Gamma}_1 = \frac{\Gamma_1 + \Gamma_2}{\sqrt{2}}$, $\tilde{\Gamma}_2 = \frac{\Gamma_2 - \Gamma_1}{\sqrt{2}}$, $\tilde{\Gamma}_3 = \frac{\Gamma_3 + \Gamma_4}{\sqrt{2}}$, and $\tilde{\Gamma}_4 = \frac{\Gamma_3 - \Gamma_4}{\sqrt{2}}$, Eq. (S10) is rewritten as

$$\mathcal{H}(k_x, k_y) = g_1(k_x) \tilde{\Gamma}_1 + g_2(k_y) \tilde{\Gamma}_2 + g_3(k_x) \tilde{\Gamma}_3 + g_4(k_y) \tilde{\Gamma}_4. \quad (\text{S11})$$

Here we have $\{\tilde{\Gamma}_i, \tilde{\Gamma}_j\} = 0$, which obey the anticommutation relation of the Clifford algebra. Equation (S11) becomes a similar separable form to Eq. (S6). Hence, the topological charges are written as

$$\mathcal{C}_n = \text{sgn}[\mathbf{J}_{\mathbf{h}_m}(\varrho_n)] = \text{sgn} \begin{bmatrix} \partial_{k_x} g_1(k_x) & 0 \\ 0 & \partial_{k_y} g_2(k_y) \end{bmatrix} \quad (\text{S12})$$

and the corresponding charge polarizations are $\mathcal{P}_n = \text{sgn}[\mathbf{P}(\varrho_n)]$ with

$$\mathbf{P}(\mathbf{k}) = \int \mathbf{J}_{\mathbf{h}_{\text{so}}}(\mathbf{k}) dk_x dk_y = \int \partial_{k_x} g_3(k_x) \partial_{k_y} g_4(k_y) dk_x dk_y = g_3(k_x) g_4(k_y). \quad (\text{S13})$$

It is clear that the second-order topology of the Hamiltonian (S10) can be characterized by $W = \sum_n \mathcal{C}_n \mathcal{P}_n / 4$.

C. 2D inseparable systems

For certain 2D inseparable systems described by

$$\mathcal{H}(\mathbf{k}) = h_1(\mathbf{k})\Gamma_1 + h_2(\mathbf{k})\Gamma_2 + h_3(\mathbf{k})\Gamma_3 + h_4(\mathbf{k})\Gamma_4, \quad (\text{S14})$$

we cannot directly deform that as the separable forms. Nevertheless, the lattice symmetries such as mirror or mirror-rotation symmetry can guarantee that the second-order topology of the inseparable $\mathcal{H}(\mathbf{k})$ is same as the 1D Hamiltonian in the high-symmetric lines, of which this 1D Hamiltonian is separable. Therefore, our proposal of W is also applicable for this inseparable $\mathcal{H}(\mathbf{k})$. Considering a inseparable Hamiltonian $\mathcal{H}(\mathbf{k})$ which has mirror-rotation symmetry M_{xy} , one can express $\mathcal{H}(\mathbf{k})$ on the high-symmetry line $k_x = k_y = k$ as

$$\mathcal{H}(k) = h_1(k)\Gamma_1 + h_2(k)\Gamma_2 + h_3(k)\Gamma_3 + h_4(k)\Gamma_4 \quad (\text{S15})$$

without changing the topology, which can be further written as

$$\mathcal{H}'(k) = H_+(k) \oplus H_-(k) \quad (\text{S16})$$

by a unitary operator $\mathcal{H}'(k) = U^{-1}\mathcal{H}(k)U$. Here $H_{\pm}(k)$ acts on the mirror-rotation subspace. The topological invariant W defined by $\mathcal{H}(\mathbf{k})$ and $\mathcal{H}'(k)$ is equivalent to the second-order topology of $\mathcal{H}(k)$. It should be noted that this inseparable system protected by M_{xy} only has the topological phase transition induced by bulk energy gap closing. We have shown these results in the second numerical example of the main text, where this 2D Hamiltonian can be firstly deformed to a form which is similar to the Hamiltonian (S11). And then, M_{xy} can drive it to the separable Hamiltonian (S15) with the same topology, which can be characterized by W .

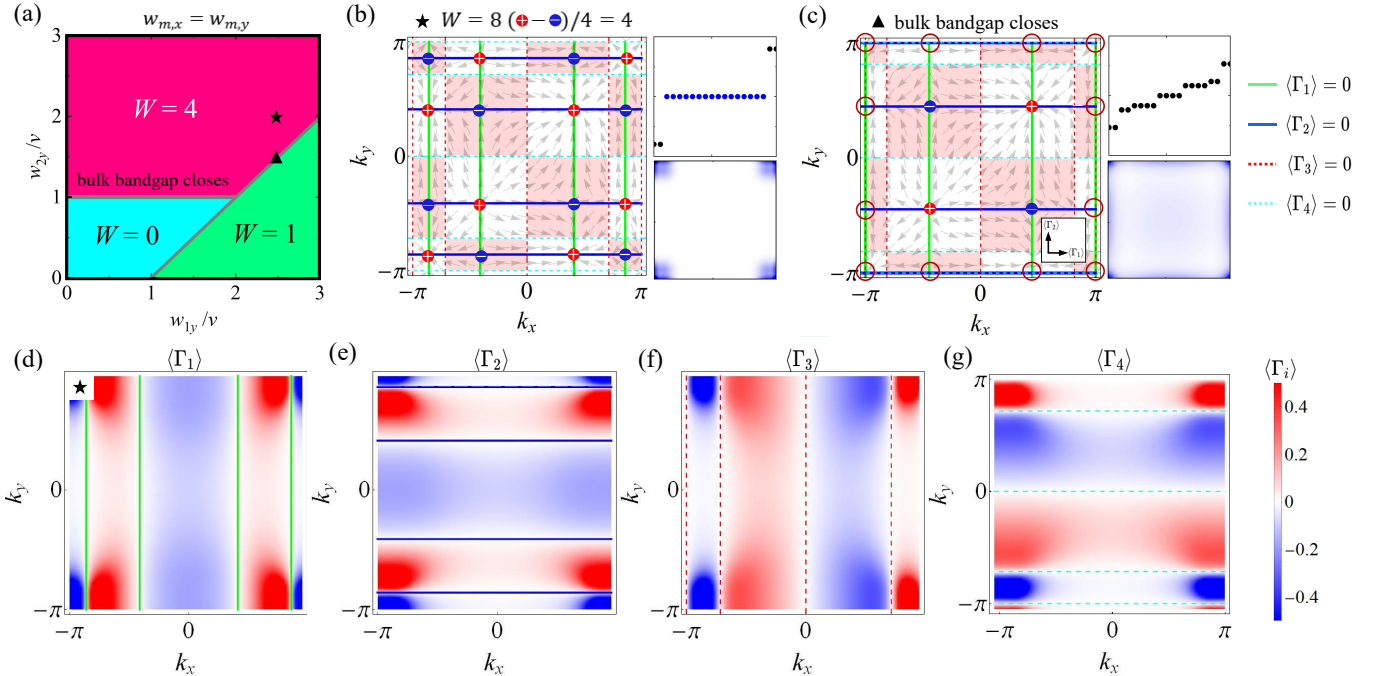


FIG. S1. (a) Phase diagrams of the second-order topological phase indicated by W . (b)-(c) Pseudospin structures of $\Theta(\mathbf{k})$, giving $W = 4$ at $w_{2,y}/v = 2.0$ (star), bulk band gap closing induced topological transitions at $w_{2,y}/v = 1.5$ (triangle), respectively. The insets show the zero-energy states at OBCs and their real-space distributions. (d)-(f) Pseudospin polarizations of $\langle \Gamma_i(\mathbf{k}) \rangle$ with $i = 1, 2, 3, 4$, where $\mathbf{h}_m = 0$ and $\mathbf{h}_{so} = 0$ are given by $\langle \Gamma_{1,2}(\mathbf{k}) \rangle$ and $\langle \Gamma_{3,4}(\mathbf{k}) \rangle$, respectively. Here the other parameters are $w_{1(2),x} = w_{1(2),y}$ and $w_{1,y}/v = 2.5$.

D. Generalization in dD d th-order topological systems

We can extend these 2D results to the dD d th-order topological phases. For the dD lattice systems hosting \mathbb{Z} -classified d th-order topological phases, the corresponding momentum-space Hamiltonian reads

$$\mathcal{H}(\mathbf{k}) = \sum_{i=1}^{2d} h_i(\mathbf{k}) \Gamma_i. \quad (\text{S17})$$

We separate \mathbf{h} -vector into two parts, i.e., $\mathbf{h} = (\mathbf{h}_m, \mathbf{h}_{so})$, where $\mathbf{h}_m = (h_1, \dots, h_d)$ describes the band dispersion and $\mathbf{h}_{so} = (h_{d+1}, \dots, h_{2d})$ denotes the SO coupling. The n th nodal point $\boldsymbol{\varrho}_n$ are determined by $\mathbf{h}_m(\boldsymbol{\varrho}_n) = 0$. Hence the polarized topological charges $\mathcal{C}_n \mathcal{P}_n$ are given by

$$\mathcal{C}_n = \text{sgn}[\mathbf{J}_{\mathbf{h}_m}(\boldsymbol{\varrho}_n)], \quad \mathbf{J}_{\mathbf{h}_m}(\mathbf{k}) = \begin{vmatrix} \partial_{k_1} h_1(\mathbf{k}) & \cdots & \partial_{k_d} h_1(\mathbf{k}) \\ \vdots & \ddots & \vdots \\ \partial_{k_1} h_d(\mathbf{k}) & \cdots & \partial_{k_d} h_d(\mathbf{k}) \end{vmatrix} \quad (\text{S18})$$

and

$$\mathcal{P}_n = \text{sgn}[\mathbf{P}(\boldsymbol{\varrho}_n)], \quad \mathbf{P}(\mathbf{k}) = \int \mathbf{J}_{\mathbf{h}_{so}}(\mathbf{k}) d\mathbf{k}. \quad (\text{S19})$$

For the typical case that $h_j(\mathbf{k})$ is a linear superposition of the k_{d+1}, \dots, k_{2d} function with $j = d+1, \dots, 2d$, we have

$$\mathbf{P}(\mathbf{k}) = h_{d+1}(\mathbf{k}) \cdots h_{2d}(\mathbf{k}). \quad (\text{S20})$$

The above results always work for the dD separable and the certain inseparable Hamiltonian similar to the above 2D cases. Hence the dD d th-order topological phases are finally determined by $1/(-2)^d$ of the total polarized topological charges in the BZ, i.e.,

$$W = \frac{1}{(-2)^d} \sum_n \mathcal{C}_n \mathcal{P}_n, \quad (\text{S21})$$

which provides an unified momentum-space characterization for the higher-order topological phases with \mathbb{Z} classification.

III. NUMERICAL RESULTS

A. Numerical results of 2D extend BBH model

We consider a 2D extended BBH model with the separable Hamiltonian [5]. The h -components are written as

$$\begin{aligned} h_1 &= v + w_{1,x} \cos k_x + w_{2,x} \cos 2k_x, \\ h_2 &= v + w_{1,y} \cos k_y + w_{2,y} \cos 2k_y, \\ h_3 &= w_{1,x} \sin k_x + w_{2,x} \sin 2k_x, \\ h_4 &= w_{1,y} \sin k_y + w_{2,y} \sin 2k_y. \end{aligned} \quad (\text{S22})$$

The Γ matrices are $\Gamma_1 = -\tau_x \sigma_z$, $\Gamma_2 = \tau_x \sigma_x$, $\Gamma_3 = -\tau_y \sigma_0$, and $\Gamma_4 = -\tau_x \sigma_y$. This system only possesses chiral symmetry under a chiral operator $\Gamma_5 = \tau_z \sigma_0$, and thus belongs to the class AIII.

When we consider the parameter of $w_{m,x} = w_{m,y}$ with $m = 1, 2$, the phase diagram indicated by W is given in Fig. S1(a). It is seen that the case of $W = 4$ is captured by sixteen polarized topological charges in Fig. S1(b), where the pseudospin polarizations of $\langle \Gamma_i(\mathbf{k}) \rangle$ with $i = 1, 2, 3, 4$ are shown in Figs. S1(d)-S1(f). Thus we can identify the values of topological charges by $\Theta(\mathbf{k})$. However, a zero-value polarized topological charge emerges at the momentum point $(-\pi, -\pi)$ when $w_{2,y} = 1.5v$ [see Fig. S1(c)], which implies that the system occurs a topological phase transition. Particularly, this topological charge is merged at the nodal point of \mathbf{h}_{so} , i.e., $\mathbf{h}_{so} = 0$, giving a bulk energy gap closing.

In addition, this system also has mirror, inversion, and C_4 -rotation symmetries with $M_x = \tau_x$, $M_y = \tau_y \sigma_y$, $I = \tau_z \sigma_y$, and $C_4 = [(\tau_x + i\tau_y)\sigma_z - (\tau_x - i\tau_y)\sigma_x]/2$ for $w_{m,x} = w_{m,y}$. This induces a twofold mirror-rotation symmetry

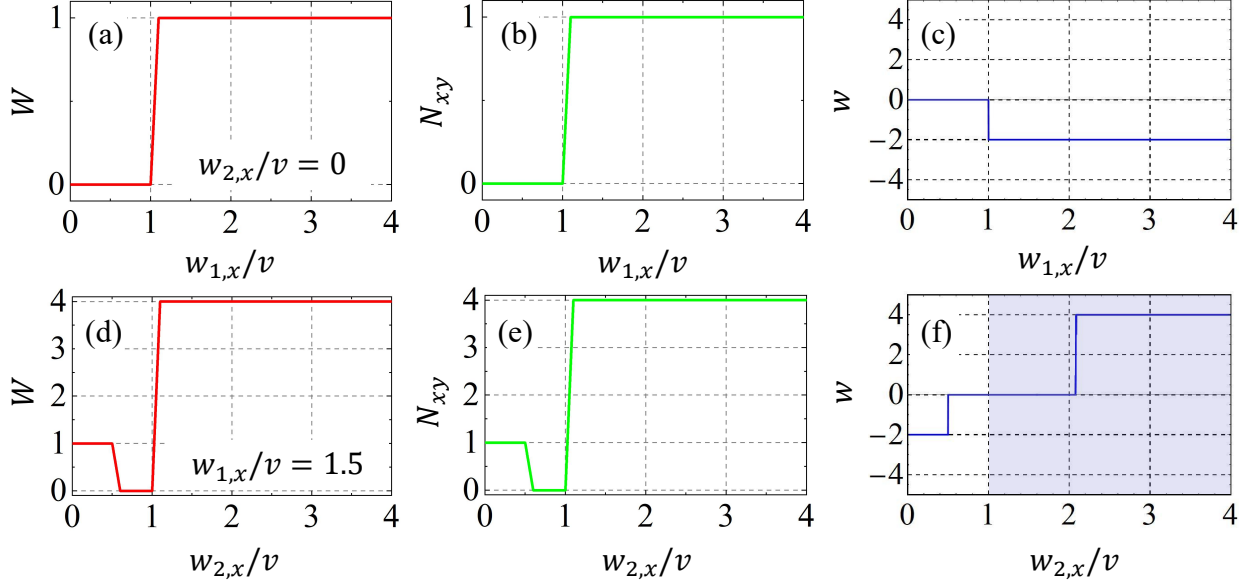


FIG. S2. The numerical results with the polarized topological charge (W), multipole chiral number (N_{xy}), and mirror-graded winding number (w). The parameters are $w_{2,x}/v = 0$ for (a), (b), and (c), and $w_{1,x}/v = 1.5$ for (d), (e), and (f). W and N_{xy} can exactly characterize the second-order topology, but w is invalid for the large-number corner states when $w_{2,x}/v > 1.0$. Here the system size is 40×40 for calculating N_{xy} .

$M_{xy}H(k_x, k_y)M_{xy}^{-1} = H(k_y, k_x)$ with $M_{xy} = C_4M_y$. Following Ref. [6], a single zero mode in each corner can be characterized by a mirror-graded winding number $w = w_+ - w_-$ with

$$w_{\pm} = \int_{\text{BZ}} \frac{dk}{4\pi i} \text{Tr} \left[S' H_{\pm}^{-1}(k) \frac{dH_{\pm}(k)}{dk} \right]. \quad (\text{S23})$$

Here we have $k_x = k_y = k$ and $H_{\pm}(k) = 2h_1\sigma_x \pm 2h_3\sigma_y$ with $S' = \sigma_z$. We show the numerical results of the different topological index in Fig. S2. It is seen that the polarized topological charge (W) and multipole chiral number (N_{xy}) can exactly characterize the second-order topology in the momentum-space and real-space, respectively. However, w is invalid for the large-number corner states, as shown in Fig. S2(f).

B. Numerical results of 2D extend BHZ model

We further consider a 2D extend Bernevig-Hughes-Zhang (BHZ) model with the inseparable Hamiltonian. The h -components read

$$\begin{aligned} h_1 &= M - 2B(2 - \cos pk_x - \cos pk_y), \quad h_3 = \sin pk_x, \\ h_2 &= (\cos 2pk_x - \cos 2pk_y), \quad h_4 = -\sin pk_y, \end{aligned} \quad (\text{S24})$$

with an integer p . The Γ matrices are given by $\Gamma_1 = \sigma_z$, $\Gamma_2 = \tau_x\sigma_x$, $\Gamma_3 = \tau_z\sigma_x$, and $\Gamma_4 = \sigma_y$, with a chiral operator $\Gamma_5 = \tau_y\sigma_x$. This Hamiltonian has time-reversal and particle-hole symmetries with $\mathcal{T} = \tau_x\mathcal{K}$ and $\mathcal{P} = \tau_z\sigma_x\mathcal{K}$, where \mathcal{K} is complex conjugate operator. Therefore, this system belongs to the class BDI. The system also hosts $M_x = \tau_y\sigma_z$, $M_y = \tau_x$, $I = \tau_z\sigma_z$, $C_4 = \text{diag}(i, 1, -1, -i)$, and $M_{xy} = C_4M_y$.

We show phase diagrams of W in Fig. S3(a). For the topological phases with $W = 1$, it is seen that the structures of $\Theta(\mathbf{k})$ figure out four polarized topological charges, as shown in Fig. S3(b), of which $\Theta(\mathbf{k})$ is determined by the pseudospin polarizations $\langle \Gamma_i(\mathbf{k}) \rangle$ with $i = 1, 2, 3, 4$ in Figs. S3(e)-S3(f). Besides, the second-order topological transitions are captured by closing bulk energy gap at the parameters $M/B = 0, 4$, and 8 , which are determined by $h_{3,4}(\varrho_n) = 0$ in Fig. S3(c) and gives $\mathcal{P}_n = 0$. This implies the value of each polarized topological charge being zero. Besides, we also show the numerical result of N_{xy} in Fig. S3(d), which is consistent with the polarized topological charges. Hence our characterization theory provides an elegant and unified scheme to identify the higher-order topological states in the momentum space.

C. Numerical results of 3D BBH model

We finally consider a simple 3D BBH model with the separable Hamiltonian $\mathcal{H}(\mathbf{k}) = \sum_{i=1}^6 h_i(\mathbf{k})\Gamma_i$ [1, 7]. The h -components read

$$\begin{aligned} h_1 &= \gamma + \lambda \cos k_x, & h_2 &= \gamma + \lambda \cos k_z, & h_3 &= \gamma + \lambda \cos k_y, \\ h_4 &= \lambda \sin k_x, & h_5 &= \lambda \sin k_y, & h_6 &= \lambda \sin k_z. \end{aligned} \quad (\text{S25})$$

The Γ matrices are given by $\Gamma_1 = \rho_x$, $\Gamma_2 = \rho_z\tau_x$, $\Gamma_3 = -\rho_z\tau_y\sigma_y$, $\Gamma_4 = -\rho_z\tau_y\sigma_z$, $\Gamma_5 = -\rho_z\tau_y\sigma_x$, and $\Gamma_6 = \rho_y$, with a chiral operator $\Gamma_7 = \rho_z\tau_z$. Here these Γ matrices obey $\text{Tr}[\Gamma_7\Gamma_1\Gamma_2\Gamma_3\Gamma_4\Gamma_5\Gamma_6] = 8i$. It is well-known that there is a quantized octupole moment $o_{xyz} = 1/2$ when $|\lambda| > |\gamma|$ [1, 7], which characterizes that this 3D system can host eight corner states and there is only one zero mode in each corner. Besides, the multipole chiral number gives $N_{xyz} = 1$ to characterize these topological states [5]. For this case of $|\lambda| > |\gamma|$, we can obtain eight topological charges

$$\mathcal{C}_n = \text{sgn}[-\lambda^3 \sin \varrho_l \sin \varrho_m \sin \varrho_s] \quad (\text{S26})$$

and their polarization

$$\mathcal{P}_n = \text{sgn}[\lambda^3 \sin \varrho_l \sin \varrho_m \sin \varrho_s], \quad (\text{S27})$$

where $\varrho_n = (\varrho_l, \varrho_m, \varrho_s)$ with $h_1(\varrho_l) = h_2(\varrho_m) = h_3(\varrho_s) = 0$ and $n = 1, 2, \dots, 8$. Here $\varrho_{l,m,s} = \pm \arccos(-\gamma/\lambda)$. Hence each polarized topological charge is given by

$$\mathcal{C}_n \mathcal{P}_n = -\text{sgn}[\lambda^6 \sin^2 \varrho_l \sin^2 \varrho_m \sin^2 \varrho_s] = -1 \quad (\text{S28})$$

and we have

$$W = -\frac{1}{8} \sum_n \mathcal{C}_n \mathcal{P}_n = 1. \quad (\text{S29})$$

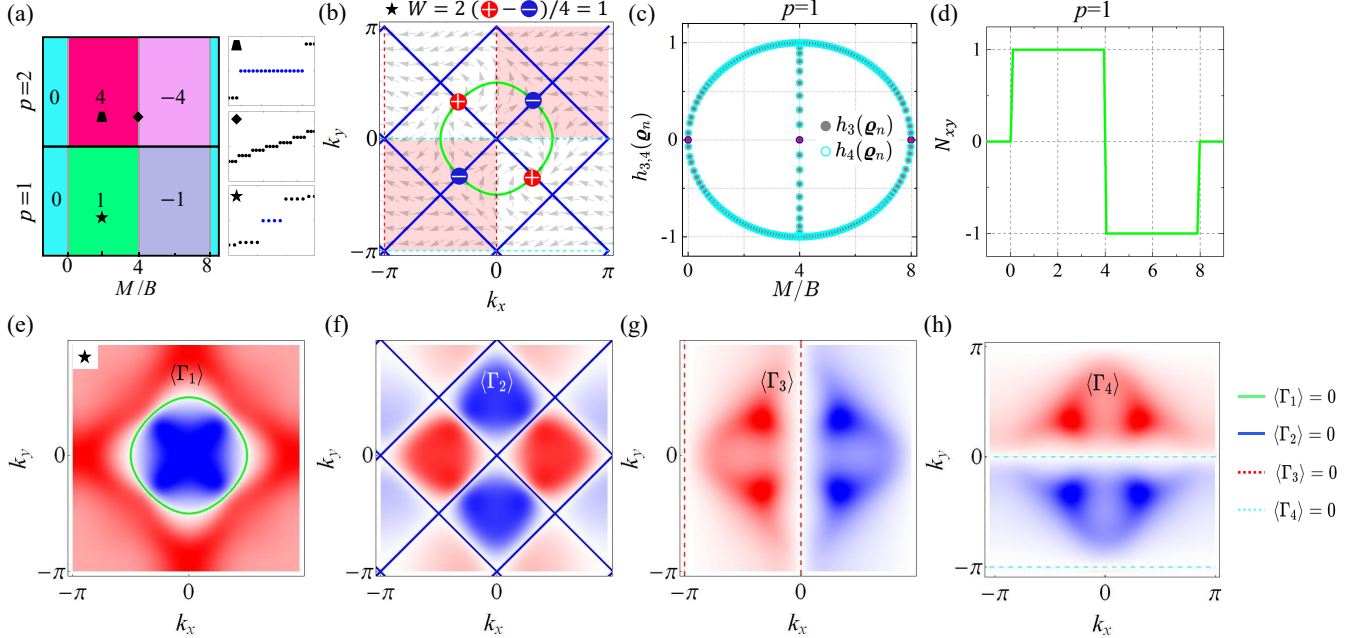


FIG. S3. (a) Phase diagrams of the second-order topological phases of the class BDI. The zero energy states of OBCs are given at the parameters $(p, M/B) = (2, 2.0)$ (trapezoid), $(2, 4.0)$ (rhombus), and $(1, 2.0)$ (star), respectively. (b) Pseudospin structures of $\Theta(\mathbf{k})$ capture four polarized topological charges, giving $W = 1$. (c) The numerical results of $h_{3,4}(\varrho_n) = 0$, giving $\mathcal{P}_n = 0$ at $M/B = 0, 4$, and 8 and showing a topological phase transition induced by bulk energy gap closing. (d) The numerical results for $p = 1$ by calculating the multipole chiral number N_{xy} with the system size 40×40 . (e)-(h) Pseudospin polarizations of $\langle \Gamma_i(\mathbf{k}) \rangle$ with $i = 1, 2, 3, 4$, where $\mathbf{h}_m = 0$ and $\mathbf{h}_{so} = 0$ are given by $\langle \Gamma_{1,2}(\mathbf{k}) \rangle$ and $\langle \Gamma_{3,4}(\mathbf{k}) \rangle$, respectively.

However, there is no topological charge for $|\lambda| < |\gamma|$, where the system is the third-order topologically trivial. For $|\lambda| = |\gamma|$, we have $\varrho_{l,m,s} = 0$ or $-\pi$, giving the topological phase transition where the bulk gap is closing. It is clear that our result W is consistent with o_{xyz} and N_{xyz} . Compared with o_{xyz} and N_{xyz} , this W is easily measured in the realistic quantum simulation experiments.

IV. HIGHER-ORDER TOPOLOGICAL PHASE TRANSITIONS

For the higher-order topological phases, it is well-known that the topological properties not only depend on the bulk topology, but can also be related to the boundary properties of the system. The main reason is that the high-dimensional boundary of the system has an open energy gap, which means that the emergence of topological phase transition can not only close the bulk energy gap but can close the boundary energy gap of different dimensions. Based on our topological characterization theory, these two types of higher-order topological transitions can be identified by the emergence of zero-polarized topological charges. Specifically, the topological charge moves to the nodal lines or surfaces of the SO field \mathbf{h}_{so} , i.e., there are N_j zero-value h_j -components with $j \in \{d+1, \dots, 2d\}$ and $0 < N_j < d$, giving a topological transition induced by boundary band gap closing. However, the topological charge moves to the nodal points of \mathbf{h}_{so} , i.e., $\mathbf{h}_{\text{so}} = 0$, giving a topological transition induced by bulk band gap closing.

For a 2D second-order topological phase described by $\mathcal{H}(\mathbf{k}) = \sum_{i=1}^4 h_i(\mathbf{k})\Gamma_i$, the topological transitions induced by bulk (edge) band gap closing can be captured by the topological charges moving to the nodal points (lines) of $\mathbf{h}_m = (h_1, h_2)$, giving $h_{1,2,3,4} = 0$ ($h_{1,3,4} = 0$ for x edge or $h_{2,3,4} = 0$ for y edge), as shown in Figs. 2(c), 2(b), and S1(c). For a 3D third-order topological phases described by $\mathcal{H}(\mathbf{k}) = \sum_{i=1}^6 h_i(\mathbf{k})\Gamma_i$, the third-order topological phase transitions are naturally identified by the zero-value polarized topological charges, giving the bulk band gap closing with $h_{1,2,3,4,5,6} = 0$, or surface band gap closing with $h_{1,2,3,4,5} = 0$ (xy surface), $h_{1,2,3,4,6} = 0$ (xz surface), and $h_{1,2,3,5,6} = 0$ (yz surface), or hinge band gap closing with $h_{1,2,3,4} = 0$ (x hinge), $h_{1,2,3,5} = 0$ (y hinge), and $h_{1,2,3,6} = 0$ (z hinge). Hence our topological characterization provides an intuitive picture to identify the higher-order topological transitions in the momentum space.

V. EXPERIMENTAL SCHEME IN ^{87}Rb ATOMIC SYSTEM

We provide an experimental scheme to realize the chiral-symmetric second-order topological phases in ^{87}Rb cold atomic system. This scheme is based on the realization of BHZ model in the recent cold atom system [8]. By employing four atomic hyperfine levels $|a\rangle = |2, -1\rangle$, $|b\rangle = |1, -1\rangle$, $|c\rangle = |2, 0\rangle$, and $|d\rangle = |1, 0\rangle$, we use the microwaves to couple $\{|a\rangle, |b\rangle\}$, $\{|c\rangle, |d\rangle\}$, $\{|a\rangle, |d\rangle\}$, and $\{|c\rangle, |b\rangle\}$ with Rabi frequencies $\Omega_1, \Omega_2, \Omega_3$, and Ω_4 . By using the bare-state basis $\{|a\rangle, |b\rangle, |c\rangle, |d\rangle\}$, the interacting Hamiltonian is given by

$$H = (\omega_a - \omega_b) |a\rangle \langle a| + (\omega_c - \omega_b) |c\rangle \langle c| + (\omega_d - \omega_b) |d\rangle \langle d| + (\Omega_1 e^{i\omega_1 t} e^{i\varphi_1} |a\rangle \langle b| + \Omega_2 e^{i\omega_2 t} e^{i\varphi_2} |c\rangle \langle d| + \Omega_3 e^{i\omega_3 t} e^{i\varphi_3} |a\rangle \langle d| + \Omega_4 e^{i\omega_4 t} e^{i\varphi_4} |c\rangle \langle b| + H.c.) \quad (\text{S30})$$

where ω_j are the energy frequencies of $|j\rangle$ with $j = a, b, c, d$. Here Ω_s, ω_s , and φ_s with $s = 1, 2, 3, 4$ are the Rabi frequencies, frequencies, and phase of the controlling microwaves, respectively. By turning the Hamiltonian to the reference frame $U = e^{-i\omega_1 t} |a\rangle \langle a| + |b\rangle \langle b| + e^{-i\omega_4 t} |c\rangle \langle c| + e^{-i(\omega_1 - \omega_3)t} |d\rangle \langle d|$, we can obtain the effective Hamiltonian $H_{\text{eff}} = i\partial_t U^\dagger U + U^\dagger H U$ as

$$H_{\text{eff}} = \begin{pmatrix} -\Delta_1 & \Omega_1 e^{-i\varphi_1} & 0 & \Omega_3 e^{-i\varphi_3} \\ \Omega_1 e^{i\varphi_1} & 0 & \Omega_4 e^{i\varphi_4} & 0 \\ 0 & \Omega_4 e^{-i\varphi_4} & -\Delta_4 & \Omega_2 e^{-i\Delta' t} e^{-i\varphi_2} \\ \Omega_3 e^{i\varphi_3} & 0 & \Omega_2 e^{i\Delta' t} e^{i\varphi_2} & \Delta_3 - \Delta_1 \end{pmatrix}, \quad (\text{S31})$$

where $\Delta_1 = \omega_1 - (\omega_a - \omega_b)$, $\Delta_2 = \omega_2 - (\omega_c - \omega_d)$, $\Delta_3 = \omega_3 - (\omega_a - \omega_d)$, $\Delta_4 = \omega_4 - (\omega_c - \omega_b)$, and $\Delta' = \omega_1 + \omega_2 - \omega_3 - \omega_4 = \Delta_1 + \Delta_2 - \Delta_3 - \Delta_4$, respectively. In order to arrive at the second-order topological phases of the class BDI, we choose $\Delta' = 0$, i.e., $\Delta_1 + \Delta_2 = \Delta_3 + \Delta_4$, which induce a time-independent Hamiltonian. We further tune $\Delta_1 = \Delta_2 = \Delta_3 = \Delta_4 = 2\Delta$ by sweeping $\omega_{1,2,3,4}$ and shift the energy levels by Δ to obtain

$$H_{\text{eff}} = \begin{pmatrix} -\Delta & \Omega_1 e^{-i\varphi_1} & 0 & \Omega_3 e^{-i\varphi_3} \\ \Omega_1 e^{i\varphi_1} & \Delta & \Omega_4 e^{i\varphi_4} & 0 \\ 0 & \Omega_4 e^{-i\varphi_4} & -\Delta & \Omega_2 e^{-i\varphi_2} \\ \Omega_3 e^{i\varphi_3} & 0 & \Omega_2 e^{i\varphi_2} & \Delta \end{pmatrix}. \quad (\text{S32})$$

In realistic experiments, we have

$$\Omega_1 = -\Omega_2 = \sqrt{h_3^2 + h_4^2}, \quad \Omega_3 = \Omega_4 = h_2, \quad \Delta = -h_1, \quad \varphi_1 = -\varphi_2 = \arctan(h_4/h_3), \quad \varphi_3 = \varphi_4 = 0. \quad (\text{S33})$$

The effective Hamiltonian in experimental conditions can be arrived at

$$H_{\text{eff}} = \begin{pmatrix} h_1 & h_3 - ih_4 & 0 & h_2 \\ h_3 + ih_4 & -h_1 & h_2 & 0 \\ 0 & h_2 & h_1 & -h_3 - ih_4 \\ h_2 & 0 & -h_3 + ih_4 & -h_1 \end{pmatrix} = h_1\sigma_z + h_2\tau_x\sigma_x + h_3\tau_z\sigma_x + h_4\sigma_y. \quad (\text{S34})$$

Compared with the experiment of realizing BHZ model, it is seen that the \mathbf{k} -dependent h_2 term opens band gap of the helical states and induces the corner states, rendering the second-order topological phases.

-
- [1] W. A. Benalcazar, B. A. Bernevig, and T. L. Hughes, Quantized electric multipole insulators, *Science* **357**, 61 (2017).
 - [2] F. Liu and K. Wakabayashi, Novel topological phase with a zero berry curvature, *Phys. Rev. Lett.* **118**, 076803 (2017).
 - [3] R. Okugawa, S. Hayashi, and T. Nakanishi, Second-order topological phases protected by chiral symmetry, *Phys. Rev. B* **100**, 235302 (2019).
 - [4] L. Trifunovic and P. W. Brouwer, Higher-Order Topological Band Structures, *Phys. Status Solidi B* **258**, 2000090 (2021).
 - [5] W. A. Benalcazar and A. Cerjan, Chiral-Symmetric Higher-Order Topological Phases of Matter, *Phys. Rev. Lett.* **128**, 127601 (2022).
 - [6] T. Liu, Y.-R. Zhang, Q. Ai, Z. Gong, K. Kawabata, M. Ueda, and F. Nori, Second-order topological phases in non-Hermitian systems, *Phys. Rev. Lett.* **122**, 076801 (2019).
 - [7] W. A. Benalcazar, B. A. Bernevig, and T. L. Hughes, Electric multipole moments, topological multipole moment pumping, and chiral hinge states in crystalline insulators, *Phys. Rev. B* **96**, 245115 (2017).
 - [8] Q.-X. Lv, Y.-X. Du, Z.-T. Liang, H.-Z. Liu, J.-H. Liang, L.-Q. Chen, L.-M. Zhou, S.-C. Zhang, D.-W. Zhang, B.-Q. Ai, *et al.*, Measurement of spin Chern numbers in quantum simulated topological insulators, *Phys. Rev. Lett.* **127**, 136802 (2021).